Conway, C.E., et al., 2020, Rapid assembly of high-Mg andesites and dacites by magma mixing at a continental arc stratovolcano: Geology, v. 48, https://doi.org/10.1130/G47614.1

Data Repository

Supplemental Analytical Methods

From the 56 samples that were identified as HMAD lavas based on whole-rock geochemistry (Conway et al., 2016; Fig. DR1), 14 were selected for this micro-analytical investigation to represent the ranges in eruption age, composition, distribution and cooling rate (Table DR2). Mineral and glass major element data were collected from thin sections of the samples using a JEOL JXA8230 SuperProbe electron probe microanalyzer (EPMA) at the National Museum of Nature and Science, Japan. The EPMA was calibrated using natural mineral standards, and synthetic standards for elements with relatively low concentrations in samples. The probe voltage and current were adjusted according to the phase: olivine and spinel (20 kV, 20 nA); clinopyroxene and orthopyroxene (15kV, 20 nA); plagioclase and hornblende (15 kV, 12 nA). A focused beam diameter was used for olivine, pyroxene, plagioclase and hornblende, and was spread to 3 μm for spinel. Secondary standards were analyzed to monitor precision and accuracy of the results. Sample and standard analytical data are available in Table DR3.

Reverse-zoned orthopyroxenes within Ruapehu HMAD lavas justify the criterion for accurate Fe-Mg interdiffusion timescale modelling recommended by Krimer and Costa (2017). Backscattered electron (BSE) images were collected based on the strong negative linear relationship between values of BSE image greyscale intensity and Mg# of orthopyroxene that has been demonstrated in previous studies (e.g. Allan et al., 2013). The relationship validates that zoning patterns observed in BSE images of orthopyroxene crystals reflect their Fe-Mg contents and can thus be used to examine compositional gradients at a higher spatial resolution than can be obtained from spot analyses (Allan et al., 2013). BSE images were collected for crystal zone boundaries suitable for diffusion modelling using a Fine 2 scanning mode at a magnification of x1,500. Following the methodology of Allan et al. (2013), we used the Image-J processing program (https://imagej.nih.gov/ij/) to rotate images so that profiles of the averaged BSE greyscale intensity were extracted perpendicular to the zoning boundary for the selected areas. These boundaries were extracted away from crystal corners, as close to perpendicular to the c-axis as possible, and have concentration plateaux at either end (see Krimer and Costa, 2017). An initial condition of a step function was assumed for all profiles. The formula of Allan et al. (2013), based on the experimental

calibration of Ganguly and Tazzoli (1994) was modified to remove an oxygen fugacity component (after Dohmen et al., 2016) and correct for a numerical error (Allan et al., 2017) to calculate $D_{Fe\text{-}Mg}$ in orthopyroxene (cf. Cooper et al., 2017):

$$log_{10}D_{Fe-Mg} = -5.54 + 2.6X_{Fe} - \frac{12{,}530}{T},$$

where X_{Fe} is the molar proportion of the Fe end member (ferrosilite) and T is temperature in Kelvins. To use this equation to yield a modelled timescale, finite difference methods were used, as detailed in Allan et al. (2013). All extracted profiles were tested to show statistical significance. The statistical significance of profiles was established by accounting for uncertainty of BSE images – related to random thermal noise of the BSE detector – scaling to $\frac{1}{\sqrt{n}}$ – where n is the number of pixels being averaged together over the profile. This yields a standard error (SE) on BSE greyscale intensities. If diffusion is the cause of the concentration profile, the plateaux at the ends of the profiles should be flat. From the 54 crystal boundaries that were modeled, we did not find any profiles that had a variation in the plateaux that exceeded 2 SE.

The orientations of crystallographic axes for 34 of the modeled orthopyroxene crystals were determined using a HITACHI SU-3500 scanning electron microscope (SEM) equipped with an Oxford Instruments HKL NordlysNano electron backscatter diffraction (EBSD) system and AZtec Software at the Geological Survey of Japan. Before SEM analysis, surface damage was removed from the thin sections by polishing them for several minutes with a Buehler VibroMet2 vibratory polisher using Syton fluid. The SEM was operated at an accelerating voltage of 15 kV in low-vacuum mode, with specimens set at a working distance of ~20 mm and tilt angle of 70°. All EBSD data were obtained using automatic indexing with a step size of 1.5-10 μm. All index data represent points with a mean angular deviation (MAD) of <1°. We performed EBSD data analyses using the AZtecHKL Channel5 Tango for mapping data and MATLAB® toolbox MTEX Version 4.5.2 (Mainprice et al., 2014) for calculating the orientations of the crystallographic axes.

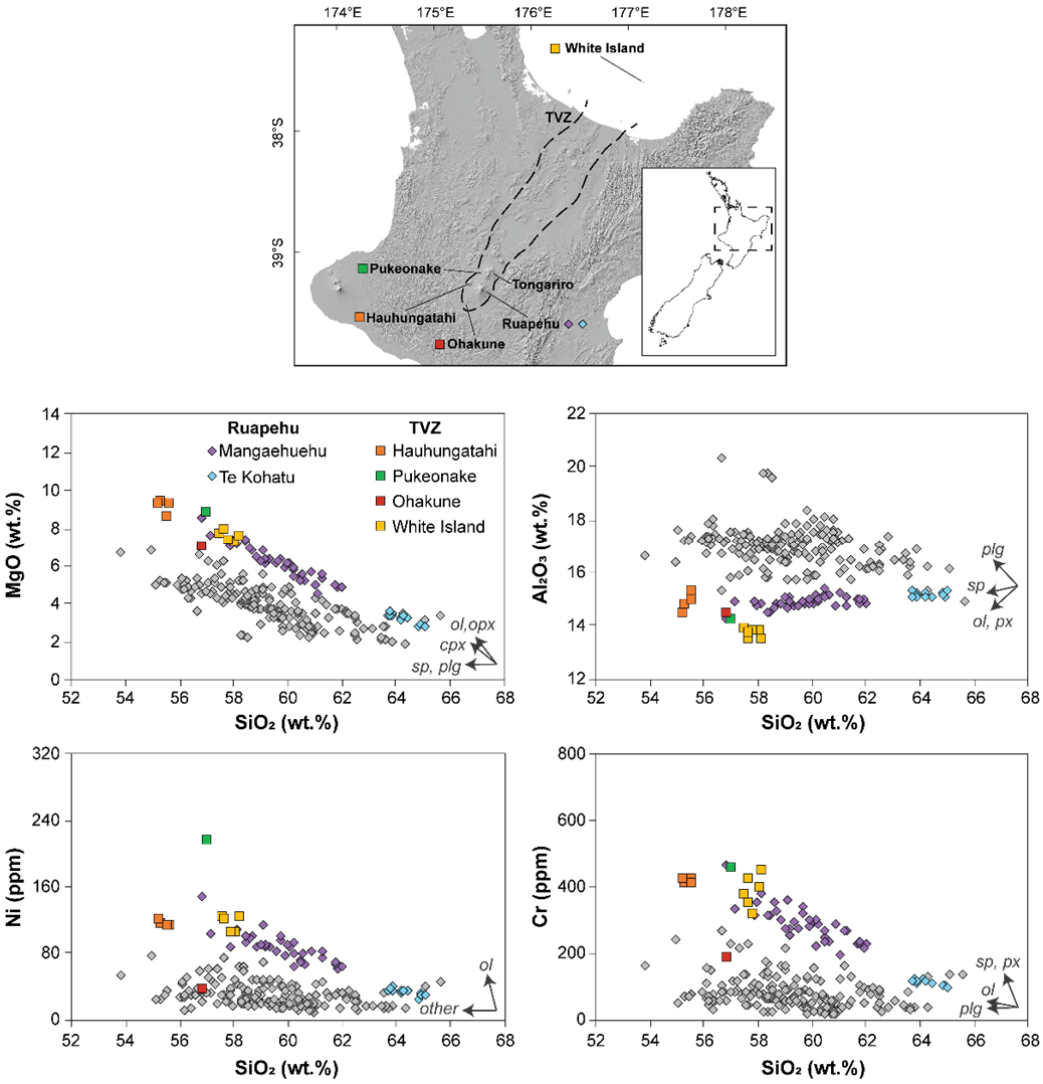

Figure DR1. Bivariate whole-rock major element diagrams for lavas from Ruapehu volcano (data from Conway et al., 2018) and HMAD volcanic rocks of the Taupo Volcanic Zone: Pukeonake, Ohakune (Graham and Hackett, 1987); Hauhungatahi (Cameron et al., 2010); and White Island (Heyworth et al., 2007). Approximate trends for accumulation of olivine (ol), orthopyroxene (opx), clinopyroxene (cpx), plagioclase (plg) and spinel (sp) are shown by the arrows.

Table DR2. Summary of data for Ruapehu HMAD lava samples used in this study.

Sample	Type	Vent	Age (ka)	2σ	SiO_2	MgO	Al_2O_3	Cr	Ni	Mg#	ol (%)
CC125	h	<2 km			56.80	8.61	14.25	470	148	69	5
***CC089**	h	<2 km	46.3	2.0	58.69	6.86	14.80	327	101	66	3
***CC174**	g	>2 km			58.84	6.55	14.83	303	87	65	3
CC540	g	>5 km			59.01	6.32	15.05	277	91	64	3
CC069	g	<2 km			59.32	6.42	14.73	300	87	65	3
CC077	g	<2 km			60.08	6.14	14.79	297	88	65	3
***CC140**	h	<2 km	42.7	1.8	60.22	5.87	14.89	287	81	64	2
***CC154**	g	>2 km			60.86	5.71	14.71	288	83	64	3
CC119	h	<2 km	44.2	1.6	61.28	5.42	15.06	270	75	63	2
***CC127**	h	<2 km	43.7	1.0	61.77	5.05	15.00	235	69	62	2
[#]CC451	h	<2 km	39.9	1.4	63.89	3.39	15.25	110	36	56	1
[#]CC415	g	<2 km	39.9	1.4	64.19	3.18	15.19	119	35	55	1
CC479	g	<2 km			64.86	2.89	15.25	103	26	54	1
CC483	g	<2 km			64.87	2.99	15.11	103	30	54	1

Notes. Geochemistry and geochronology data are from Conway et al. (2016) and Ingham et al. (2017). Mineral diffusion timescales have been modeled for samples marked by (*). Eruption age for samples marked by ([#]) is taken from sample CC414 from the same lava flow. Type displays whether a sample has a holocrystalline (h) or glassy (g) groundmass texture; the former is produced by relatively prolonged cooling of the lava after its emplacement and the latter results from relatively rapid quenching. Vent displays the distance to the inferred eruptive vent location from the sample collection point. Whole-rock major oxide values are in weight %, normalized to anhydrous totals of 100 %. Cr and Ni contents are in ppm. Whole-rock Mg# values (100xMg/(Mg+Fe)) and olivine contents (%) show a general positive correlation.

Table DR3. EPMA mineral chemistry dataset (link to Excel file)

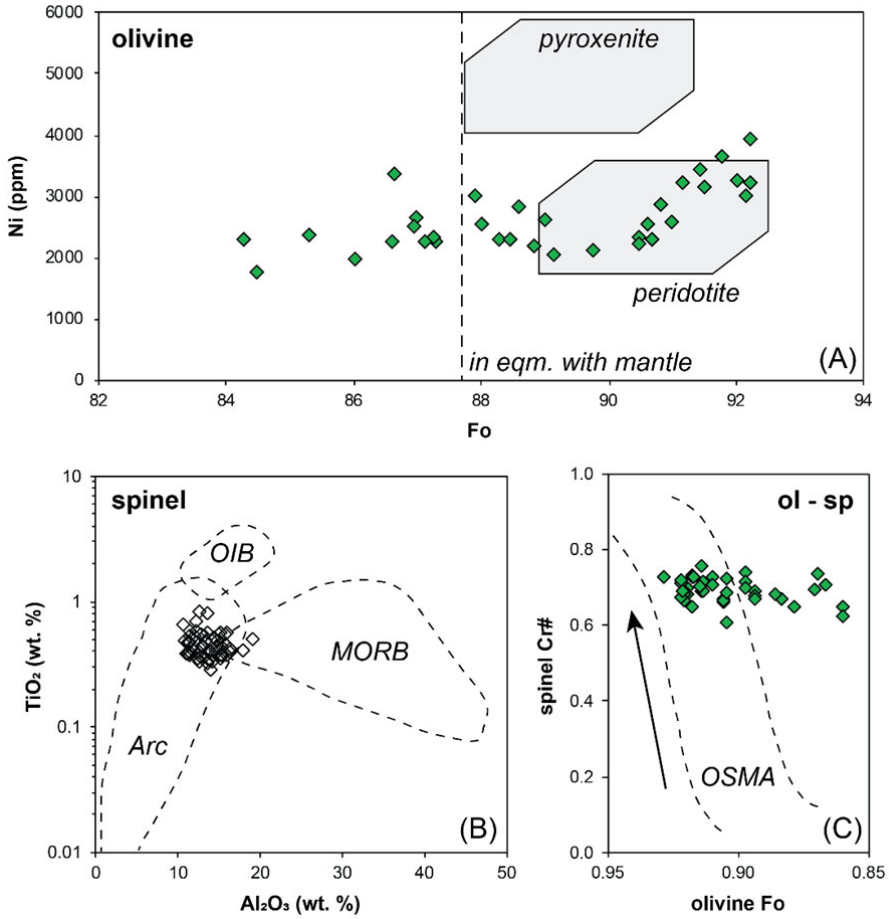

Figure DR4. Geochemistry data for Type 4 olivine and spinel crystals in Ruapehu high-Mg andesites and dacites. (A) Ni vs. Fo (100xMg(Mg+Fe)) plot for olivines. Shaded fields are from Sobolev et al. (2005) and Straub et al. (2011). (B) TiO_2 vs. Al_2O_3 plot for spinels. Fields are from Kamenetsky et al. (2001). (C) Cr# of spinel vs. Fo of olivine for Type 4 olivines with spinel inclusions. Paired crystal analyses are compared with the olivine-spinel mantle array (OSMA) defined by Arai (1994). The arrow points towards increasing mantle depletion. Together, these data indicate that Type 4 olivines were sourced from depleted arc peridotite beneath Ruapehu.

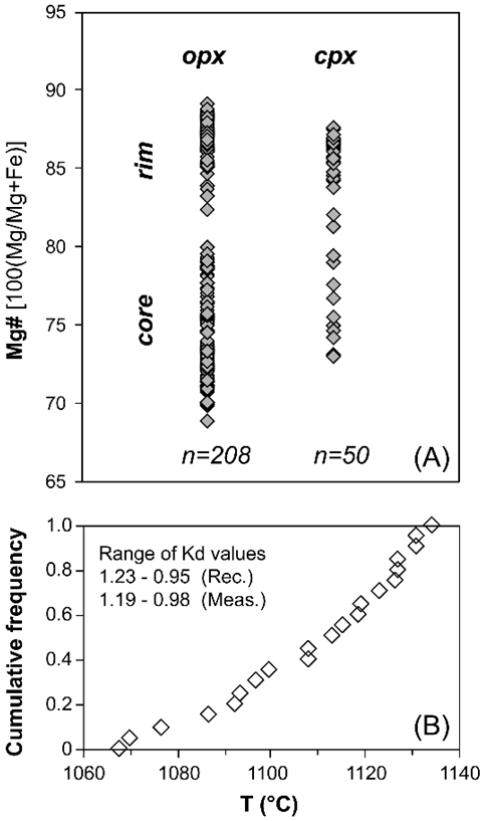

Figure DR5. Geochemistry and geothermometry data for Type 1 pyroxene crystals from Ruapehu high-Mg andesites and dacites. (A) Mg# values for core and rim analyses of Type 1 orthopyroxene (opx) and clinopyroxene (cpx) crystals. (B) Results from application of the two-pyroxene geothermometer of Putirka (2008) to pairs of rims for Type 1 orthopyroxene and clinopyroxene. The measured range (Meas.) for values of Kd is compared with the recommended range (Rec.) provided by Putirka (2008).

REFERENCES CITED IN DATA REPOSITORY

Allan, A.S.R., Morgan, D.J., Wilson, C.J.N., and Millet, M.-A., 2013, From mush to eruption in centuries: assembly of the super-sized Oruanui magma body: Contributions to Mineralogy and Petrology, v. 166, p. 143–164, https://doi.org/10.1007/s00410-013-0869-2.

Allan, A.S.R., Barker, S.J., Millet, M.-A., Morgan, D.J., Rooyakkers, S.J., Schipper, C.I., and Wilson, C.J.N., 2017, A cascade of magmatic events during the assembly and eruption of a super-sized magma body: Contributions to Mineralogy and Petrology, v. 172, 49, https://doi.org/10.1007/s00410-017-1367-8.

Arai, S., 1994, Characterization of spinel peridotites by olivine-spinel compositional relationships: review and interpretation. Chemical Geology, v. 113, p. 191–204, https://doi.org/10.1016/0009-2541(94)90066-3.

Cameron, E., Gamble, J.A., Price, R.C., Smith, I.E.M., McIntosh, W., Gardner, M., 2010, The petrology, geochronology and geochemistry of Hauhungatahi volcano, S.W. Taupo Volcanic Zone: Journal of Volcanology and Geothermal Research v. 190, p. 179–191.

Conway, C.E., Leonard, G.S., Townsend, D.B., Calvert, A.T., Wilson, C.J.N., Gamble, J.A., and Eaves, S.R., 2016, A high-resolution $^{40}Ar/^{39}Ar$ lava chronology and edifice construction history for Ruapehu volcano, New Zealand: Journal of Volcanology and Geothermal Research, v. 327, p. 152–179, https://doi.org/10.1016/j.jvolgeores.2016.07.006.

Conway, C.E., Gamble, J.A., Wilson, C.J.N., Leonard, G.S., Townsend, D.B., Calvert, A.T., 2018, New petrological, geochemical, and geochronological perspectives on andesite-dacite magma genesis at Ruapehu volcano, New Zealand: American Mineralogist, v. 103, p. 565–581, http://doi.org/10.2138/am-2018-6199.

Cooper, G.F., Morgan, D.J., and Wilson, C.J.N., 2017, Rapid assembly and rejuvenation of a large silicic magmatic system: insights from mineral diffusive profiles in the Kidnappers and Rocky Hill deposits, New Zealand: Earth and Planetary Science Letters, v. 473, p. 1–13, http://dx.doi.org/10.1016/j.epsl.2017.05.036.

Dohmen, R., Ter Heege, J.H., Becker, H.-W., and Chakraborty, S., 2016, Fe–Mg interdiffusion in orthopyroxene: American Mineralogist, v. 101, p. 2210–2221, https://doi.org/10.2138/am-2016-5815.

Ganguly, J., and Tazzoli, V., 1994, Fe^{2+}–Mg interdiffusion in orthopyroxene: Retrieval from the data on intracrystalline exchange reaction: American Mineralogist, v. 79, p. 930–937.

Graham, I.J, and Hackett, W.R., 1987, Petrology of calc-alkaline lavas from Ruapehu Volcano and related vents, Taupo Volcanic Zone: Journal of Petrology, v. 28, p. 531–567, https://doi.org/ 10.1093/petrology/28.3.531.

Heyworth, Z., Turner, S., Schaefer, B., Wood, B., George, R., Berlo, K., Cunningham, H., Price, R., Cook, C., and Gamble, J., 2007, ^{238}U–^{230}Th–^{226}Ra–^{210}Pb constraints on the genesis of high-Mg andesites at White Island, New Zealand: Chemical Geology, v. 243, p. 105–121, https://doi.org/10.1016/j.chemgeo.2007.05.012.

Kamenetsky, V.S., Crawford, A.J., and Meffre, S., 2001, Factors controlling chemistry of magmatic spinel: an empirical study of associated olivine, Cr-spinel and melt inclusions from primitive rocks: Journal of Petrology, v. 42, p. 655–671, https://doi.org/10.1093/petrology/42.4.655.

Krimer, D., and Costa, F., 2017, Evaluation of the effects of 3D diffusion, crystal geometry, and initial conditions on retrieved time-scales from Fe-Mg zoning in natural oriented orthopyroxene crystals: Geochimica et Cosmochimica Acta, v. 196, p. 271–288, https://doi.org/10.1016/j.gca.2016.09.037.

Mainprice, D., Bachmann, F., Hielscher, R., and Schaeben, H., 2014, Descriptive tools for the analysis of texture projects with large datasets using MTEX: strength, symmetry and components, *in* Faulkner, D.R., Mariani, E., and Mecklenburgh, J., eds., Rock deformation from field, experiments, and theory: A Volume in Honour of Ernie Rutter: Geological Society of London, Special Publication, v. 409, p. 251–271, https://doi.org/10.1144/SP409.8

Putirka, K.D., 2008, Thermometers and barometers for volcanic systems: Reviews in Mineralogy and Geochemistry, v. 69, p. 61–120, https://doi.org/10.2138/rmg.2008.69.3.

Sobolev, A.V., Hofmann, A.W., Sobolev, S.V., and Nikogosian, I.K., 2005, An olivine-free mantle source of Hawaiian shield basalts: Nature, v. 434, p. 590–597, https://doi.org/10.1038/nature03411.

Straub, S.M., Gomez-Tuena, A., Stuart, F.M., Zellmer, G.F., Espinasa-Perena, R., Cai, Y., and Iizuka, Y., 2011. Formation of hybrid arc andesites beneath thick continental crust: Earth and Planetary Science Letters, v. 303, p. 337–347, https://doi.org/10.1016/j.epsl.2011.01.013.